American Mineralogist, Volume 103, pages 1435–1444, 2018

# Kuliginite, a new hydroxychloride mineral from the Udachnaya kimberlite pipe, Yakutia: Implications for low-temperature hydrothermal alteration of the kimberlites

Denis S. Mikhailenko[1,*,†], Andrey V. Korsakov[1], Sergey V. Rashchenko[1,2], Yurii V. Seryotkin[1,2], Dmitriy I. Belakovskiy[3], and Alexander V. Golovin[1]

[1]V.S. Sobolev Institute of Geology and Mineralogy of the Siberian Branch of the RAS, 3, Akademika Koptyuga Avenue, Novosibirsk 630090, Russia
[2]Department of Geology and Geophysics, Novosibirsk State University, 1 Pirogova Street, 630090 Novosibirsk, Russia
[3]Fersman Mineralogical Museum, Russian Academy of Sciences, Leninskiy Prospekt 18 korp. 2, Moscow 119071, Russia

## Abstract

Kuliginite is a new iron-magnesium hydroxychloride mineral with the ideal formula $Fe_3Mg(OH)_6Cl_2$ from the Udachnaya East kimberlite, Yakutia, Russia. It occurs as green prismatic-bipyramidal crystals (0.2–0.5 mm) and fills cavities and veins in several units of kimberlites together with iowaite, gypsum, calcite, halite, barite, and celestine. It is trigonal, with $R\bar{3}$ space group. Kuliginite has imperfect cleavage on $\{10\bar{1}1\}$. The spinel-like crystal structure of kuliginite is also typical for several copper minerals of the atacamite group with common formula $Cu_3M(OH)_6Cl_2$; kuliginite can be regarded as a $Fe^{2+}$ analog of tondiite [$Cu_3Mg(OH)_6Cl_2$].

The occurrence of the kuliginite + iowaite + gypsum assemblage has implications for the interpretation of low-temperature (below 100°C) hydrothermal processes and alteration of kimberlite by hydrothermal fluids/brines, as well as for transport of metals in Cl-bearing solutions. This secondary hydrothermal mineral assemblage formed much later than the kimberlite groundmass minerals. Kuliginite contains inclusions of iowaite indicating their simultaneous crystallization.

**Keywords:** New mineral, kuliginite, crystal structure, kimberlite, atacamite group, hydroxychloride; Dynamics of Magmatic Processes

## Introduction

The Paleozoic Udachnaya kimberlite pipe is the world's largest diamond deposit, and it is located in the Yakutsk diamond province in the central Siberian craton. It has a complex structure (Kharkiv et al. 1998), with several distinct "volcanoclastic units" and "coherent" kimberlite in each pipe (Fig. 1), according to the modern model (Smith et al. 2013).

Na-K-Cl-bearing minerals were found in various assemblages from different units of the Udachnaya East kimberlite, but the source of Na and Cl in these units remains poorly constrained. Melt inclusion studies (Golovin et al. 2003, 2007, 2017; Kamenetsky et al. 2004, 2006, 2007b, 2009, 2014; Mernagh et al. 2011), as well as Sr, Nd, and Pb isotopes (Maas et al. 2005; Kamenetsky et al. 2009, 2014) and sulfur isotope data (Kitayama et al. 2017) on the Udachnaya-East rocks provide solid proofs for magmatic mantle origin of the Na-K-Cl component in two non-serpentinized ultra-fresh units of the Udachnaya East kimberlite. Thus, the discovery of these two compositionally unusual units offers a unique opportunity to study the composition and evolution of kimberlitic magma (Golovin et al. 2017; Kamenetsky et al. 2007b, 2012, 2014; Kitayama et al. 2017). On the other hand, some authors argue that any assemblage with chlorides larger than 1 cm in any unit of the Udachnaya East kimberlite from the depths of 410–640 m may be evaporatic or xenoliths coming from the host sediments (Kopylova et al. 2016).

This paper presents new data on mineral assemblages containing chlorides in voids from several types of kimberlites originated at the depths of 560–640 m in the Udachnaya East pipe, where a new hydroxychloride mineral, kuliginite, was found. Kuliginite is a new iron-magnesium hydroxychloride (IMA 2016-049) that belongs to the atacamite group (Hålenius et al. 2016) and was named after Sergey Semenovich Kuligin, Russian geologist and researcher (1961–2014), who for years studied Yakutian kimberlites, xenoliths, and alluvial diamond deposits all over Yakutia in search for unknown kimberlite pipes. S.S. Kuligin, together with his colleagues from the Sobolev Institute of Geology and Mineralogy (IGM, Novosibirsk, Russia), discovered the Nicka diamondiferous placer along the Tyung River (Yakutia). The holotype sample of kimberlite with abundant kuliginite is stored in the collection of the Central Siberian Geological Museum of IGM under the number VI-53/1.

## Analytical techniques

Mineral chemistry of kuliginite (40 chemical analyses, Table 1), iowaite, celestine, and calcite were determined in IGM using a JEOL JXA-8100 electron microprobe operated at 20 kV acceleration voltage, 5 μm beam diameter, 50 nA focused beam current, and 20–30 s counting time; TESCAN MIRA 3 LMU JSM 6510LV equipped with an Oxford Instruments INCA energy-dispersive detector was used for chemical mapping at the operating conditions 20 kV, 1 nA, with an interval of 0.78 s for each spot.

Raman spectra in the range from 50 to 4000 $cm^{-1}$ were collected with a Horiba Jobin Yvon LabRam HR800 Laser Raman spectrometer, using a 532 nm laser, at

* E-mail: pazilovdenis@igm.nsc.ru
† Special collection papers can be found online at http://www.minsocam.org/MSA/AmMin/special-collections.html.

0003-004X/18/0009–1435$05.00/DOI: http://doi.org/10.2138/am-2018-6363

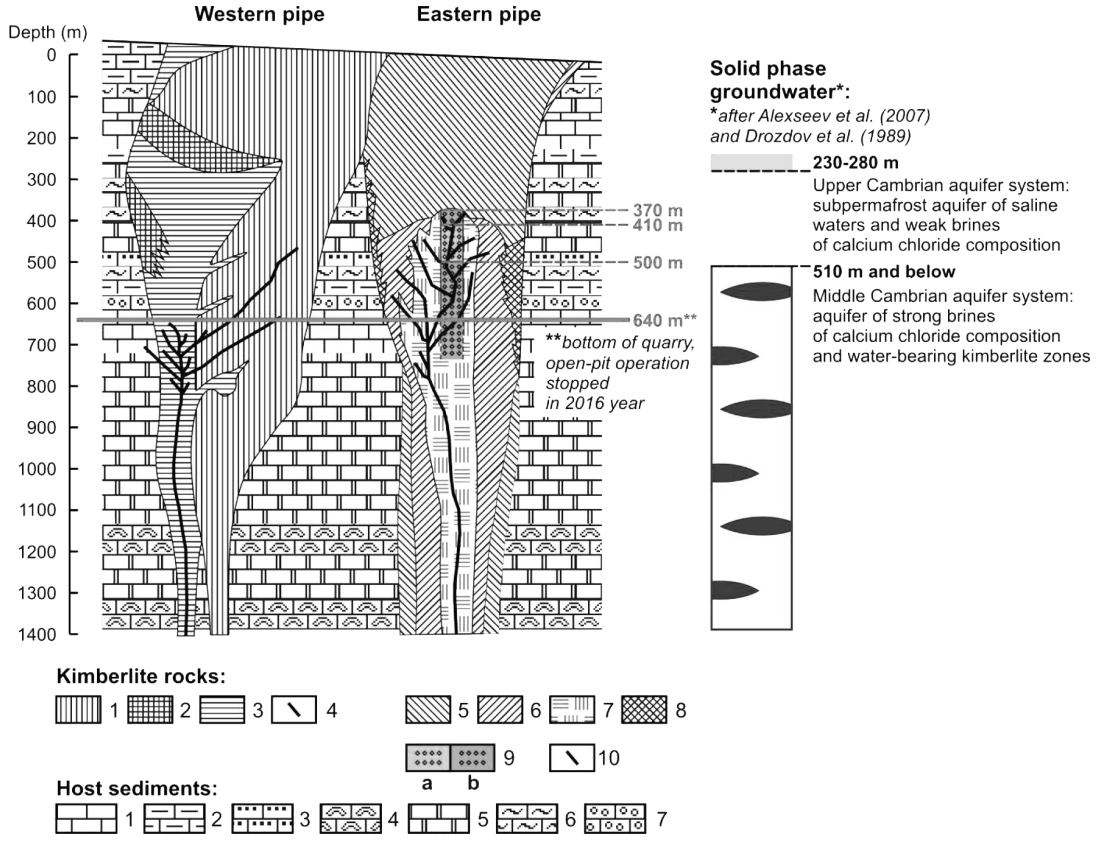


**Figure 1.** Geological section of the Udachnaya kimberlite pipe according to Kryuchkov and Sviridov [modified by Golovin et al. (2017) after Fig. 47 from Kharkiv et al. (1998)]. 1–4 = Western body with volcaniclastic kimberlite (1–3; separated units, which have well-defined boundaries) and veins of coherent kimberlite (4). 5–10 = Eastern body consisting of volcaniclastic kimberlite (5–9, separated units), and veins of coherent kimberlites (10). Volcaniclastic kimberlite (9). (**a**) Green = unserpentinized fresh kimberlites [for details see Kamenetsky et al. (2012, 2014)], the 410–500 m depth interval. (**b**) Rusty = partially serpentinized kimberlites at 370–410 and 500–640 m. The upper boundary for kimberlites (9) at 370 m is according to Kharkiv et al. (1998) and Marshintsev et al. (1976); other boundaries were constrained during 2003–2016 fieldwork in the quarry. Host sediments [after Alekseev (2009)]: limestones (1 = clear, 2 = silty, 3 = sandy, 4 = organogenic), dolomites (5), marls (6), and calcareous conglomerates (7).

15 mW (spot size of about 0.8 μm) coupled with an Olympus microscope with an LMPLFLN100x long-working distance objective (focal length 640 mm).

A 0.56 × 0.37 × 0.08 mm$^3$ single crystal of kuliginite was selected for single-crystal X-ray diffraction using a polarizing microscope. X-ray diffraction data were collected on an Oxford Diffraction Gemini R Ultra single-crystal diffractometer (CCD-detector, graphite-monochromatized Mo$K\alpha$ radiation) using an ω-scan technique with the scan width of 1° per frame. Data reduction with numeric and empirical absorption corrections was performed using Rigaku Oxford Diffraction CrysAlisPro software. Space group $R\bar{3}$ was selected on the basis of $R_{int}$ (4.18% for $R3$, 7.36% for $R3m$), the choice was then supported by analysis of $wR$ values (see below). JANA 2006 software (Petrıcek et al. 2014) including SUPERFLIP program (Palatinus and Chapuis 2007) was used for structure solution and refinement. Coordinates of all atomic positions except hydrogen (M1, M2, O1, and Cl1) were obtained from charge flipping. Coordinates of the remaining hydrogen position (H1) were extracted from a Fourier difference map. Anisotropic displacement parameters were refined for all atomic positions except isotropically refined hydrogen. A refinement of Fe/Mg proportion in M1 and M2 sites resulted in $Fe_{0.97}Mg_{0.03}$ occupancy of M1 site, and $Mg_{0.85}Fe_{0.15}$ occupancy of M2 site, giving the formula $Fe_{3.04}Mg_{0.96}(OH)_6Cl_2$, consistent the formula derived from the chemical analyses, $Fe_{2.98}Mn_{0.11}Mg_{0.91}(OH)_6Cl_2$ (note that Fe and Mn cannot be separated on the basis of X-ray diffraction). Bond-valence calculations (Table 2) confirm that $Fe^{2+}$ and $Mn^{2+}$ should preferentially occupy M1 site, and $Mg^{2+}$the M2 site.

Crystal data, data collection, and structure refinement details are summarized in Supplemental[1] Table 1; fractional atomic coordinates and isotropic or equivalent isotropic displacement parameters are summarized in Supplemental[1] Table 2 (see the CIF in Supplemental[1] materials).

A powder X-ray diffraction pattern of kuliginite (Fig. 2) was measured using a DRON diffractometer (Bragg-Brentano geometry, Cu$K\alpha$ radiation). Main diffraction peaks are listed in Supplemental[1] Table 3.

## Geological setting

The Udachnaya kimberlite pipe consists of two kimberlite bodies at the surface: East and West Udachnaya kimberlites (Kharkiv et al. 1998). The Udachnaya East kimberlite has a U-Pb age of 367 ± 5 Ma, and the age of the West body is in a range of 353–359 Ma (Kinny et al. 1997), but its separate units (possibly, phases) have never been dated (Fig. 1). As shown by $^{40}Ar/^{39}Ar$ dating of phlogopite from kelyphitic rims around garnet from Udachnaya East kimberlite pipe (Yudin et al. 2011), the kimberlite magma of the western body intruded later and affected thermally the already formed kimberlites of the eastern pipe.

The Udachnaya kimberlite intruded Lower Ordovician (exposed on the surface) and Middle and Upper Cambrian (obtained from drilling) dolomite, limestone, marl, mudrocks, siltstone, and sandstone and encloses xenoliths of limestone and

**Table 1.** Chemical composition (wt%) of different minerals occurring together with kuliginite from Udachnaya kimberlite pipe (C = center; R = rim)

| | Kuliginite | Detection limits | Avg. (n = 40) | St.dev. (n = 40) | Iowaite | Iowaite | Celestine |
|---|---|---|---|---|---|---|---|
| | C | | | | C | R | C |
| $SiO_2$ | 0.00 | 0.052 | 0.02 | 0.02 | b.d. | 0.36 | b.d. |
| $Al_2O_3$ | 0.01 | 0.015 | 0.01 | 0.02 | 0.6 | 0.51 | b.d. |
| FeO | 57.7 | 0.013 | 57.3 | 0.26 | 24.5 | 24.7 | b.d. |
| MnO | 2.26 | 0.012 | 2.14 | 0.13 | b.d. | b.d | b.d. |
| MgO | 9.79 | 0.018 | 9.68 | 0.39 | 36.8 | 34.3 | b.d. |
| CaO | 0.02 | 0.007 | 0.01 | 0.01 | b.d. | 0.69 | b.d. |
| $Na_2O$ | 0.01 | 0.013 | 0.02 | 0.02 | 0.23 | 0.63 | b.d. |
| $K_2O$ | 0.00 | 0.006 | 0.00 | 0.01 | b.d. | 0.12 | b.d. |
| Cl | 19.3 | 0.016 | 19.3 | 0.24 | 10.7 | 9 | b.d. |
| F | 0.11 | 0.015 | 0.15 | 0.03 | b.d. | b.d. | b.d. |
| $P_2O_5$ | 0.03 | 0.020 | 0.02 | 0.02 | b.d. | b.d. | b.d. |
| SrO | b.d. | 0.011 | – | – | b.d. | b.d. | 44.1 |
| BaO | 0.02 | 0.018 | 0.01 | 0.01 | b.d. | b.d. | 12.7 |
| $SO_3$ | 0.00 | 0.008 | 0.01 | 0.01 | b.d. | b.d. | 43.3 |
| $H_2O$* | 11.6 | – | – | – | – | – | – |
| Total | 100.8 | – | – | – | 72.8 | 70.2 | 100.0 |

*Notes:* b.d. = below detection limit; dash = not analyzed. $H_2O$* = calculated from structural data.

**Table 2.** Bond lengths for M1 and M2 sites in kuliginite structure and corresponding bond-valence sums (BVSs) for different cations (Brese and O'Keeffe 1991)

| | | | |
|---|---|---|---|
| M1-O1 | 2.0477(9) | M2-O1 | 2.1029(11) |
| M1-O1 | 2.0477(9) | M2-O1 | 2.1029(12) |
| M1-O1 | 2.1466(14) | M2-O1 | 2.1029(12) |
| M1-O1 | 2.1466(14) | M2-O1 | 2.1029(11) |
| M1-Cl1 | 2.6363(5) | M2-O1 | 2.1029(12) |
| M1-Cl1 | 2.6363(5) | M2-O1 | 2.1029(12) |
| bvs for $Fe^{2+}$ | **1.93** | | 2.21 |
| bvs for $Mg^{2+}$ | 1.8 | | **1.98** |
| bvs for $Mn^{2+}$ | 2.27 | | 2.58 |

dolomite with minor amounts of clayey and sandy material, as well as marl and siltstone, no younger than Devonian (Davis et al. 1980; Brakhfogel 1984; Kinny et al. 1997).

There are several units of kimberlites within the Udachnaya system (Fig. 1; Kharkiv et al. 1998). The western body is strongly serpentinized all along the exposed depth of 1400 m (Kharkiv et al. 1998), while the eastern body comprises two non-serpentinized units (Fig. 1, units 9a and 10), at depths below 370 m and at least four units serpentinized to different degrees, with different contents of olivine and olivine/serpentine ratios (Fig. 1).

Volcanoclastic and coherent non-serpentinized kimberlites from the depths 410–500 m (Fig. 1, units 9a and 10) contain chlorides, alkali carbonates, and alkali sulfates and sulfides in the groundmass (Kamenetsky et al. 2007b, 2009, 2012, 2014; d'Eyrames et al. 2017), as well as the so-called chloride and chloride-carbonate nodules reaching 30 cm in diameter, which are uncommon in other kimberlites worldwide. The chloride nodules are composed mainly of halite and sylvite, while the chloride-carbonate ones consist of chlorides, calcite, and a series of Na-Ca carbonates [shortite $Na_2Ca_2(CO_3)_3$], nyerereite $(Na,K)_2Ca(CO_3)_2$, and northupite $[Na_3Mg(CO_3)_2Cl]$ and a minor amount of aphthitalite $[K_3Na(SO_4)_2]$ (Kamenetsky et al. 2006, 2007a, 2014).

The host sediments include several aquifers. One deep aquifer system has its top at 510 m below the surface and stores strong brines of a calcium chloride composition and water-bearing kimberlite zones (Drozdov et al. 1989; Alexeev et al. 2007). All kimberlites below 510 m contain neither chloride and chloride-carbonate nodules nor assemblages of chlorides with alkali carbonates and sulfates in the groundmass, and all units of the Udachnaya East kimberlite within the 510–640 m depths are more or less strongly serpentinized. At the same time, both volcaniclastic and coherent kimberlites between 560 and 640 m include later mineral assemblages with halite and sylvite that

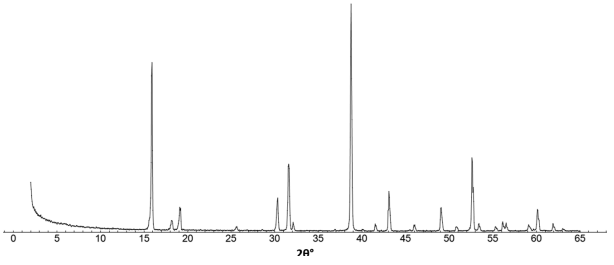


**Figure 2.** Powder X-ray diffraction pattern of kuliginite (Cu*K*α radiation).

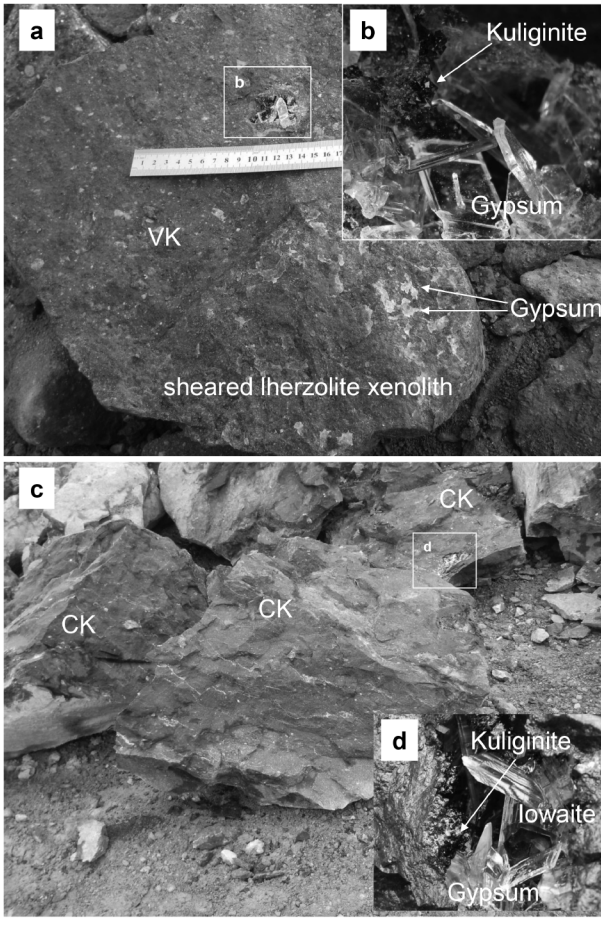


**Figure 3.** (**a**) Volcaniclastic (VK) and (**c**) coherent (CK) kimberlites from Udachnaya-East pipe. VK and CK correspond to unit 9b and, respectively, from Figure 1. (**b**) Kuliginite with gypsum in the void from VK. (**d**) Paragenesis of kuliginite, iowaite, and gypsum in the lens from CK.

fill veins, fractures, and voids and can reach tens of centimeters in size (Fig. 3).

## Occurrence and mineral associations of kuliginite

Kuliginite and iowaite, together with other minerals, were found in cavities or veins in weakly serpentinized volcaniclastic and coherent kimberlites of the Udachnaya East pipe below 560 m. The amount of xenolithic material from the sediment host is moderate in volcaniclastic kimberlite (~15 vol%, Fig. 3), which constitutes a separate unit in the central part of the East pipe below 510 m (Fig. 1, units 9b), and low in coherent kimberlite (~5 vol%, Fig. 4a, unit 10 in Fig. 1), which is a dike in xenolith-rich (~50 vol%) volcaniclastic kimberlite (unit 7 in Fig. 1) exposed at the depth about 560 m in the southwestern part of the Udachnaya East kimberlite.

Kuliginite was identified as euhedral prismatic-bipyramidal crystals (0.2–0.5 mm) (Fig. 4b) in aggregates with iowaite, calcite, as inclusions in halite (Figs. 3 and 4), and also together with gypsum and barite (Figs. 3 and 5b). Kuliginite crystals are green (Fig. 3) and some are coated by a red rust-like phase as a result of $Fe^{2+}$ oxidation (Figs. 3a and 3b). The following crystallization sequence of minerals was observed: serpentine → calcite → kuliginite + iowaite + halite + barite + calcite + gypsum → halite (Fig. 6). Note that abundant kuliginite and iowaite inclusions occur in centers of halite lenses or veins in kimberlite. Both kuliginite and iowaite crystals become coarser from toward the vein center. Kuliginite slowly dissolves in $H_2O$ at room temperature but oxidizes very fast upon interaction with atmospheric water even at ambient humidity. The empirical formula, based on four cations per formula unit (pfu), is $(Fe_{2.98}Mn_{0.02})(Mg_{0.91}Mn_{0.09})(OH_{5.95}F_{0.03}Cl_{0.02})Cl_2$. The ideal end-member formula is $Fe_3Mg(OH)_6Cl_2$.

Coarse (2–3 cm), dark green pseudohexagonal iowaite crystals in the Udachnaya kimberlite are intergrown with elongate prismatic crystals of gypsum and kuliginite or enclosed in halite

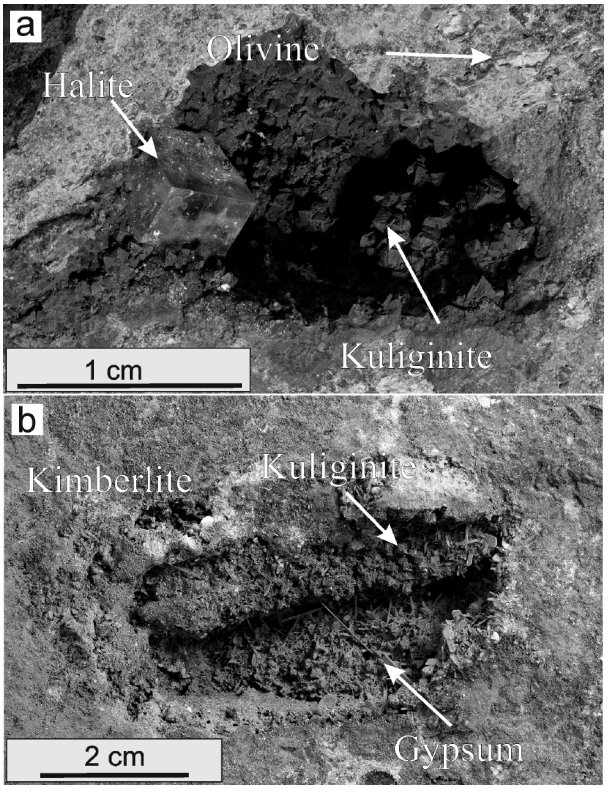


**Figure 5.** (**a**) Geode with a colorless halite and kuliginite crystal. (**b**) Photograph of geode with gypsum and kuliginite in kimberlite.

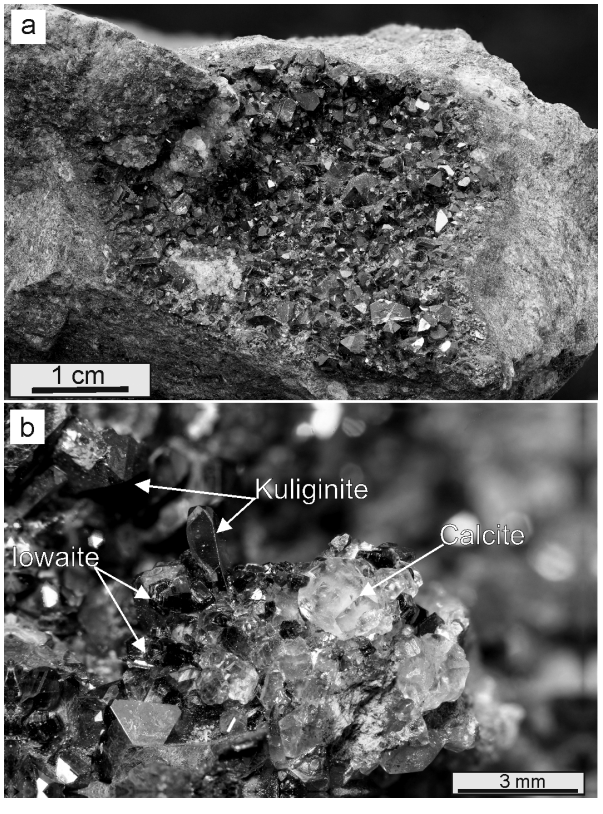


**Figure 4.** (**a**) Geode of kuliginite, iowaite, and calcite in the Udachnaya East kimberlite pipe. (**b**) Photo of green transparent kuliginite crystals coexisting with dark green iowaite and white calcite crystals.

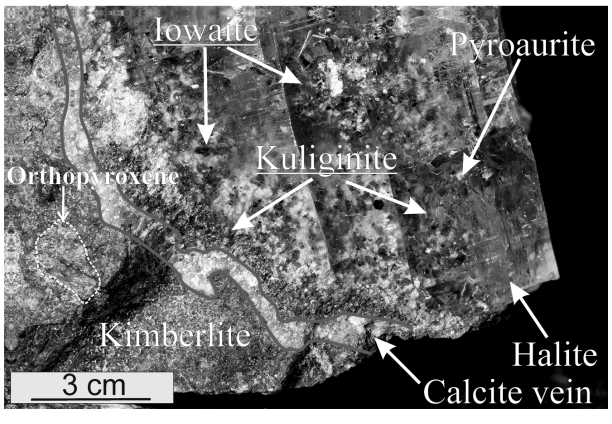


**Figure 6.** Contact of kimberlite and halite nodules with red rust iowaite.

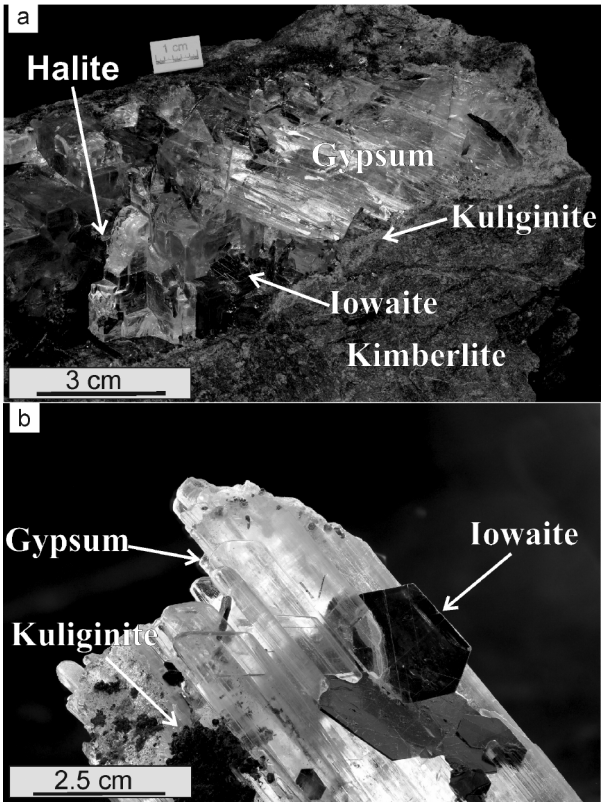


**Figure 7.** (**a**) Gypsum and iowaite crystals in halite from the Udachnaya East kimberlite pipe. (**b**) Photo of gypsum and iowaite crystal.

and gypsum (Figs. 3 and 7). The crystals are free from features of dissolution. Some iowaite [$Mg_6Fe^{3+}_2(OH)_{16}Cl_2 \cdot 4H_2O$] has transformed into brown-gilded pyroaurite [$Mg_2Fe_2CO_3(OH)_6 \cdot 4H_2O$] under sunlight (Fig. 3d). The Udachnaya iowaite markedly differs in mineral chemistry from its synthetic counterparts (Frost et al. 2005) and natural analogs (Braithwaite et al. 1994). The chemical composition of iowaite is shown in Table 3.

Elongate prisms of gypsum (up to 20 cm long) bear abundant visible inclusions of other minerals (iowaite, halite, etc.). Gypsum is either intergrown with or enclosed in halite (single inclusions), which also hosts anhydrite inclusions with up to 2.3 wt% SrO.

Massive euhedral crystals of halite, reaching 10 cm grown together with elongate gypsum prisms (Figs. 3a, 3d, and 7a) and enclose gypsum, kuliginite, and celestine. Halite contains minor amounts of impurities, below the detection limit, and $H_2O$ fluid inclusions marked by a Raman peak at 3446 $cm^{-1}$ (Fig. 8b).

Celestine grains are either euhedral or anhedral. Euhedral grains (up to 2.5 cm in size) were identified in a large gypsum crystal (up to 7 cm in size), and anhedral celestines (up to 80–90 μm in size) occur as inclusions in halite. The composition of celestine approaches stoichiometry, but many grains contain 9.6 to 13.6 wt% BaO (Table 3).

Carbonates in the studied mineral assemblage are represented only by calcite (with 0.5–0.7 wt% SrO) found as inclusions in halite and syngenetic intergrowths with kuliginite.

**Table 3.** Comparison of Raman peaks of kuliginite with those of $Fe_2(OH)_3Cl$ and their assignment according to Reguer et al. (2007)

| Raman bands of kuliginite | $Fe_2(OH)_3Cl$ (Reguer et al. 2007) | Suggested assigment |
|---|---|---|
| 129 | 127 | – |
| – | 160 | O-Fe-O bending mode |
| 207 | 200 | – |
| 282 | – | – |
| – | 318 | Fe-Cl stretching vibration |
| 445 | 423 | Fe-O stretching vibration |
| 610 | 618 | – |
| 676 | – | Mg-O stretching vibration |
| – | 804 | Hydroxyl deformation mode |
| 3551 | 3552 | Hydroxyl stretching vibration |

## Physical properties

Kuliginite crystals (0.5 mm) are dark green, transparent, and non-pleochroic in transmitted light. Some grains (or grain parts) are greenish-yellow, obviously due to inclusions of iron oxides or hydroxides produced by alteration. Despite trigonal symmetry, the mineral shows anomalous biaxiality with $2V_{meas} = 10(5)°$ (see discussion below). Grain fragments often have somewhat rhombic shape with the acute angle close to 65°. Taking into account that rhombohedral angle of kuliginite unit cell is near 67°, one can suggest imperfect cleavage on {10$\bar{1}$1} main rhombohedron similarly to herbertsmithite and leverettite.

Kuliginite is biaxial (+), $\alpha = 1.709(3)$, $\beta = 1.709(3)$, $\gamma = 1.718$ ($\lambda = 589$ nm); dispersion of the optical axis is noticeably, $r > v$.

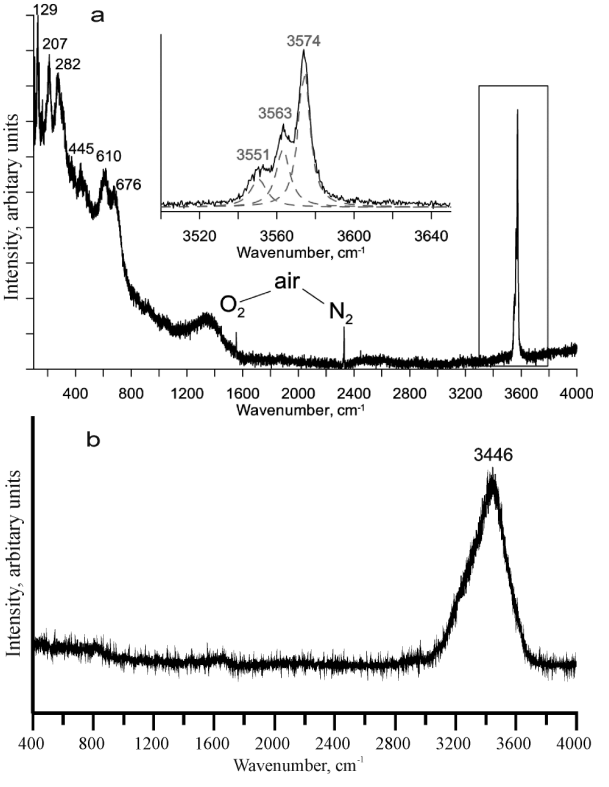


**Figure 8.** (**a**) Raman spectrum of kuliginite. See Table 4 for assignment of Raman bands. (**b**) Raman spectra of an $H_2O$ inclusion in halite.

The density of kuliginite measured by the sink-float method, using about 10 microscopically selected fragments free from inclusions, is 3.13 g/cm$^3$ ($D_{calc}$ = 3.001 g/cm$^3$); Mohs hardness is 3–3.5.

## Crystal structure

The crystal structure of kuliginite has atomic packing similar to spinel structure with vacant tetrahedral sites. Octahedral sites in the kuliginite structure are represented by "intralayer" M1 site occupied by $Fe_{0.97}Mg_{0.03}$, and "interlayer" M2 site, occupied by $Mg_{0.85}Fe_{0.15}$. The M1:M2 ratio in the crystal structure is 3:1. The M1 site is coordinated by four hydroxyl groups and two chloride anions in the opposite vertices of a slightly distorted $Fe(OH)_4Cl_2$ octahedron. These $Fe(OH)_4Cl_2$ octahedra form gibbsite-type layers parallel to the (001) plane; the chloride anions appear on the junctions of three such octahedra (Fig. 9a). The M2 site is coordinated by six hydroxyl groups and links neighboring gibbsite-type layers of M1-centered octahedra through the triple junctions (Figs. 9b–9c). The structural formula of the kuliginite is, therefore, $^{M1}(Fe_{2.89}Mg_{0.11})^{M2}(Mg_{0.85}Fe_{0.15})(OH)_6Cl_2$.

An interesting feature of kuliginite structure is a breaking of possible $R\bar{3}m$ symmetry due to slight (<0.1 Å) displacement of oxygen and hydrogen atoms from {110} planes, whereas remaining atomic sites are situated in special positions compatible with $R\bar{3}m$ (Fig. 9d, Supplemental[1] Table 1). Although the structure can be also solved in the $R3m$ space group, the resulting $wR$ factor of 7.12% (for all reflections) is considerably higher than the corresponding value of 4.83%, obtained for a solution in the $R3$ space group. An application of the Hamilton test (Hamilton 1965) to these values suggests the correctness of our space group choice within significance level of 0.005.

The chloride anions on the junctions of three M1-centered octahedra also play a role of proton acceptors for three hydroxyl groups of the adjacent gibbsite-type ring (Fig. 9d). The resulting O-H···Cl bonds are characterized by distances H···Cl of 2.39(3) Å, O···Cl of 3.2376(12) Å, and angle O-H···Cl of 162(2)°. Such parameters allow classification of these bonds as hydrogen bonds according to several dedicated studies (Mascal 1997; Aullon et al. 1998; Steiner 1998).

Although there is no systematic study of how the strength of O-H···Cl hydrogen bond affects O-H stretching frequency like that made by Libowitzky (1999) for O-H···O bonding, the observed O-H stretching frequencies of kuliginite (3550–3575 cm$^{-1}$; see Fig. 8a and Table 3) correspond to "plateau" on the Libowizky's ν(O-H)/d(O···O) plot, indicating a negligible influence of weak O-H···Cl hydrogen bonding. The observed

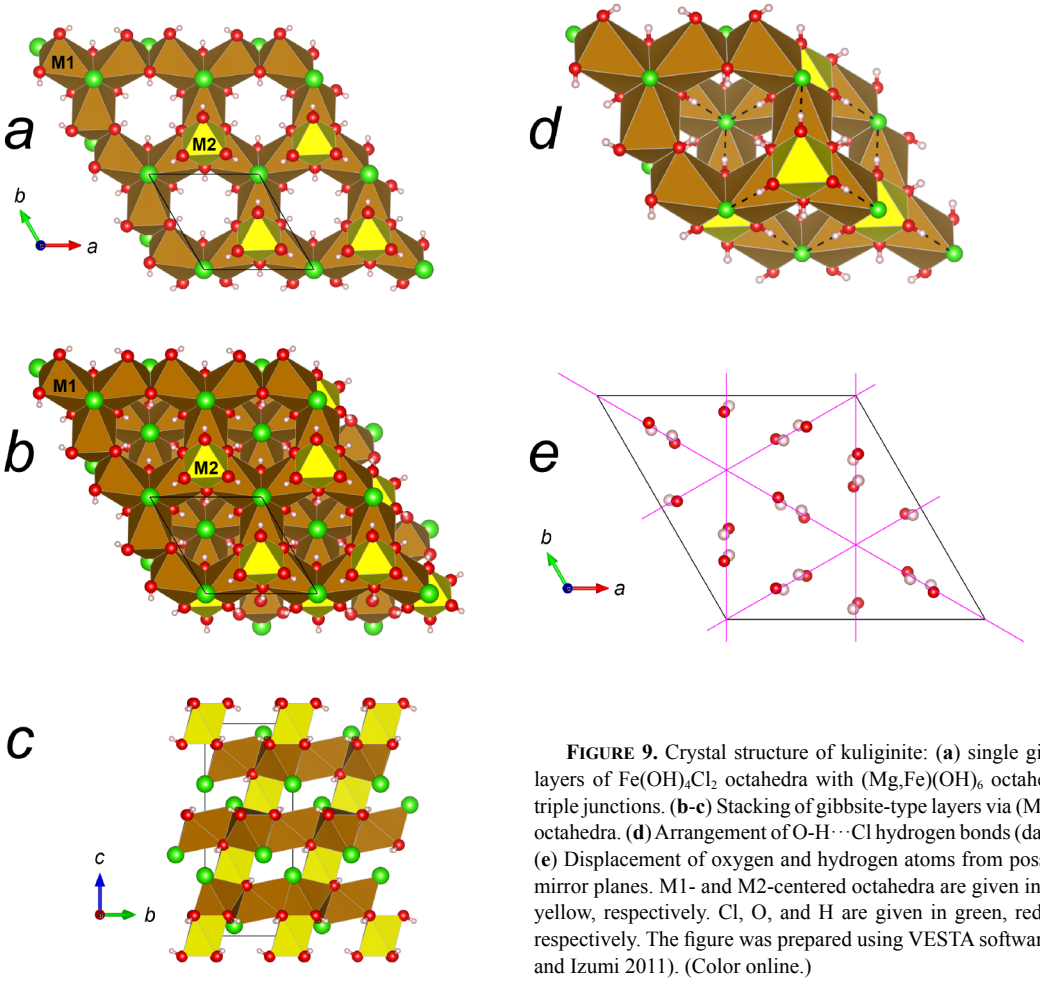


**Figure 9.** Crystal structure of kuliginite: (**a**) single gibbsite-type layers of $Fe(OH)_4Cl_2$ octahedra with $(Mg,Fe)(OH)_6$ octahedra on the triple junctions. (**b-c**) Stacking of gibbsite-type layers via $(Mg,Fe)(OH)_6$ octahedra. (**d**) Arrangement of O-H···Cl hydrogen bonds (dashed lines). (**e**) Displacement of oxygen and hydrogen atoms from possible {110} mirror planes. M1- and M2-centered octahedra are given in brown and yellow, respectively. Cl, O, and H are given in green, red, and pink, respectively. The figure was prepared using VESTA software (Momma and Izumi 2011). (Color online.)

splitting of O-H stretching frequency into three components (Fig. 8a) most probably corresponds to the Mg-for-Fe substitution in M2 site and presence of Mn in octahedral sites.

## Raman spectroscopy

### Kuliginite

Unpolarized single-crystal Raman spectra of kuliginite (Fig. 8a) show a band at 445 $cm^{-1}$ that is close to that of synthetic $Fe_2(OH)_3Cl$ and can be attributed to a Fe-O stretching mode, similarly to (Reguer et al. 2007) (Table 3). The Raman bands in the range 3600–3500 $cm^{-1}$ may be attributed to OH hydroxyl stretching vibrations (Fig. 8a).

### Iowaite

The Raman spectra of iowaite from our mineral assemblage (Fig. 10) show typical peaks at 524, 279, 437, and 101 $cm^{-1}$ (Frost et al. 2005). One spectrum contains a $CO_3$ carbonate peak at 1307 $cm^{-1}$. Other bands are observed for synthetic and natural iowaite at 3545, 3421, 3281, 3058, and 2769 $cm^{-1}$, which are assigned to the stretching vibrations of interlayer water (Frost et al. 2005).

## Discussion

### Related minerals

Kuliginite belongs to the atacamite group of hydroxychloride minerals with $M_2(OH)_3Cl$ stoichiometry, where M is a divalent cation ($Cu^{2+}$, $Mg^{2+}$, $Fe^{2+}$, $Mn^{2+}$, $Co^{2+}$, $Ni^{2+}$, $Zn^{2+}$). The members of atacamite group may be divided into two subgroups: with the brucite-like stacking of cation coordination octahedra, and with the spinel-like stacking of cation coordination octahedra (Table 4).

The spinel-like trigonal structure of kuliginite is also typical for several copper minerals of the atacamite group including herbertsmithite, gillardite, leverettite, tondiite, and paratacamites (Table 4). Kuliginite, $Fe_3Mg(OH)_6Cl_2$, herewith, can be regarded as Fe-analog of tondiite, $Cu_3Mg(OH)_6Cl_2$. The composition of kuliginite is quite similar to that of hibbingite, an orthorhombic $Fe_2(OH)_3Cl$ hydroxychloride, especially if the latter demonstrates a partial $Fe^{2+} \leftarrow Mg^{2+}$ substitution (Saini-Eidukat et al. 1994). However, the difference in symmetry results in different X-ray diffraction patterns (Fig. 11) allowing the discrimination of these species by means of X-ray diffraction. An important issue is a relation of kuliginite to atacamite mineral species. On the one hand, amakinite was described as a mineral with $Fe(OH)_2$ idealized composition and brucite-like structure (Kozlov and Levshov 1962), and herewith by no means related to kuliginite. On the other hand, the reported optical and physical properties, X-ray diffraction (Fig. 11), lattice parameters [$a$ = 6.917(3), $b$ = 14.52(1) Å], and cationic composition ($Fe_{2.92}Mg_{0.90}Mn_{0.18}$ normalized per 4 cations) of amakinite too strongly resemble those of kuliginite to be accidental. Taking into account that the crystal structure of amakinite has actually never been determined, and chemical analysis applied in 1962 probably was not able to detect chlorine we conclude that amakinite is closely related to kuliginite. Unfortunately, the holotype of amakinite was reported to be completely decomposed into rust (Dmitriy I. Belakovskiy,

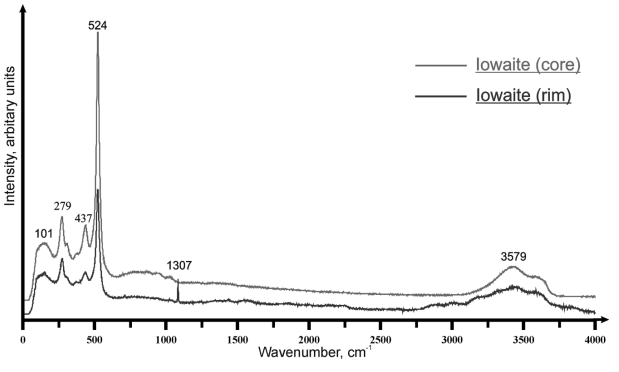


**Figure 10.** Raman spectra of iowaite.

**Table 4.** Mineral species of atacamite group (note that cation sites are separated in the formulas)

| Brucite-like stacking | Spinel-like stacking |
|---|---|
| **Monoclinic** | |
| Botallackite (Hawthorne 1985)<br>$CuCu(OH)_3Cl$, $P2_1/m$<br>$a$ = 5.717(1), $b$ = 6.126(1),<br>$c$ = 5.636(1) Å<br>β = 93.07(1)° | Clinoatacamite (Malcherek and Schlüter 2009)<br>$Cu_2CuCu(OH)_6Cl_2$, $P2_1/n$<br>$a$ = 6.1226(3), $b$ = 6.8346(4),<br>$c$ = 9.1841(6)<br>β = 99.577(4) |
| Iyoite (Nishio-Hamane et al. 2017)<br>$CuMn(OH)_3Cl$, $P2_1/m$<br>$a$ = 5.717(2), $b$ = 6.586(2), $c$ = 5.623(3) Å<br>β = 88.45(3)° [91.55(3)° in conventional setting] | |
| **Orthorhombic** | |
| | Atacamite (Parise and Hyde 1986)<br>$CuCu(OH)_3Cl$, $Pnma$<br>$a$ = 6.030 (2) $b$ = 6.865 (2), $c$ = 9.120 (2) Å |
| | Kempite (Rogers 1924)<br>$[MnMn(OH)_3Cl]$[a]<br>$a$ = 6.49, $b$ = 7.12, $c$ = 9.52 Å |
| | Hibbingite (Saini-Eidukat et al. 1994)<br>$[FeFe(OH)_3Cl]$[a]<br>$a$ = 6.31(6), $c$ = 7.10(7), $b$ = 9.20(4) Å |
| **Trigonal** | |
| Kapellasite (Krause et al. 2006)<br>$Cu_3Zn(OH)_6Cl_2$, $P\bar{3}m1$<br>$a$ = 6.300(1), $c$ = 5.733(1) Å | Herbertsmithite (Braithwaite et al. 2011)<br>$Cu_3Zn(OH)_6Cl_2$, $R\bar{3}m$<br>$a$ = 6.834(1), $c$ = 14.075(2) Å |
| Haydeeite (Malcherek and Schlüter 2007)<br>$Cu_3Mg(OH)_6Cl_2$, $P\bar{3}m1$<br>$a$ = 6.2733(4), $c$ = 5.7472(5) Å | Gillardite (Clissold et al. 2007)<br>$Cu_3Ni(OH)_6Cl_2$, $R\bar{3}m$<br>$a$ = 6.8364(1), $c$ = 13.8459(4) Å |
| Misakiite (Nishio-Hamane et al. 2017)<br>$Cu_3Mn(OH)_6Cl_2$, $P\bar{3}m1$<br>$a$ = 6.4156(4), $c$ = 5.7026(5) Å | Leverettite (Kampf et al. 2013a)<br>$Cu_3Co(OH)_6Cl_2$, $R\bar{3}m$<br>$a$ = 6.8436(6), $c$ = 14.064(1) Å |
| Centennialite (Crichton and Müller 2017)<br>$Cu_3Ca(OH)_6Cl_2{\cdot}H_2O$, $P\bar{3}m1$<br>$a$ = 6.6606(9), $c$ = 5.8004(8) Å | Tondiite (Malcherek et al. 2014)<br>$Cu_3Mg(OH)_6Cl_2$, $R\bar{3}m$<br>$a$ = 6.8377(7), $c$ = 14.088(2) Å |
| | Kuliginite<br>$Fe_3Mg(OH)_6Cl_2$, $R\bar{3}$[b]<br>$a$ = 6.9521(5), $c$ = 14.5740(11) Å |
| | Paratacamite (Welch et al. 2014)<br>$Cu_6Cu_6(Zn,Cu)_3(Zn,Cu)(OH)_{24}Cl_8$, $R\bar{3}$[c]<br>$a$ = 13.6440(4), $c$ = 14.0354(7) Å |
| | Paratacamite-(Mg) (Kampf et al. 2013b)<br>$Cu_6Cu_6(Mg,Cu)_3(Mg,Cu)(OH)_{24}Cl_8$, $R\bar{3}$[c]<br>$a$ = 13.689(1), $c$ = 14.025(1) Å |
| | Paratacamite-(Ni) (Sciberras et al. 2013)<br>$Cu_6Cu_6(Ni,Cu)_3(Ni,Cu)(OH)_{24}Cl_8$, $R\bar{3}$[c]<br>$a$ = 13.682(2), $c$ = 13.916(2) Å |

[a] Crystal structures of kempite and hibbingite have been never determined, so structural formulas are given by analogy with atacamite. Lattice parameters from original sources are transformed to the conventional setting ($a < b < c$).
[b] Pronounced $R3m$ pseudosymmetry (see Crystal structure section).
[c] Pronounced herbertsmithite-like $R\bar{3}m$ substructure with $a_s = a/2$.

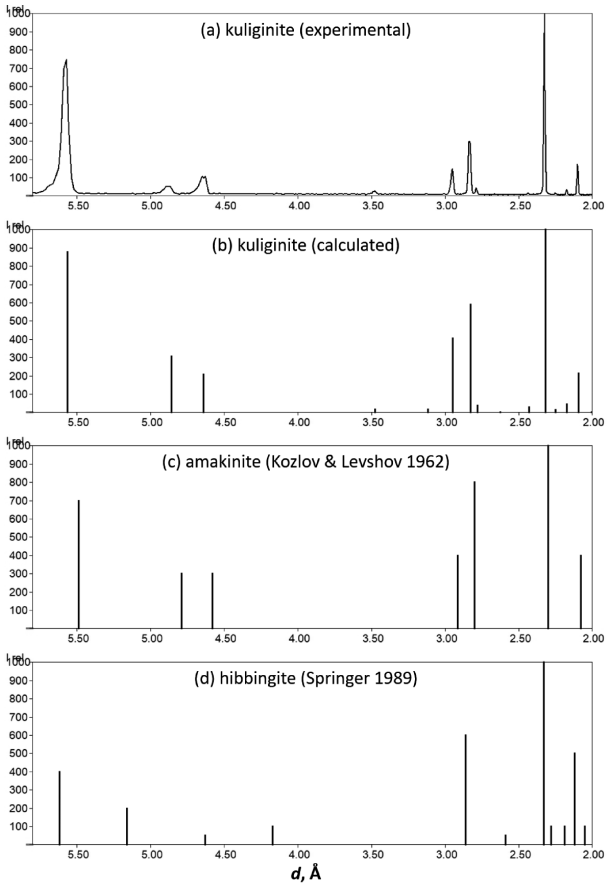


**FIGURE 11.** X-ray diffraction of kuliginite-related minerals.

Fersman Mineralogical Museum, private communication), so the verification of our hypothesis is impossible.

The mixed occupancy $Mg_{0.85}Fe_{0.15}$ of "intralayer" cation site in kuliginite also implies the existence of samples close to a Fe-dominant analog of kuliginite with idealized formula $Fe_3Fe(OH)_4Cl_2$. Such a compound with $R\bar{3}m$ space group [$a$ = 6.9594(5), $c$ = 14.7847(12) Å] was described among synthetic materials (ICSD-155535), but was not observed among minerals yet.

### Formation of the kuliginite mineral assemblages

Kuliginite is a rare phase with optic properties impeding its identification: its biaxiality is inconsistent with its trigonal symmetry observed by X-ray diffraction. Thus, the biaxial behavior must be anomalous. Anomalous optics of uniaxial compounds is relatively common and described in detail by Shtukenberg and Punin (2007). It is often observed in beryl, indialite, osumilite-group minerals, etc., and is usually due to deformation associated with stress during or after crystallization. It might also result from variations of oxidation and/or dehydration degrees in different crystal parts or atomic ordering (Foord and Mills 1978; Kahr and McBride 1992; Shtukenberg and Punin 2007).

Discovery of Cl-rich minerals, such as halite, iowaite, and kuliginite, in the weakly serpentinized Udachnaya East kimberlite is evidence of high chlorine enrichment of the growth medium, but none of these minerals have been described in the Udachnaya-East ultra-fresh low-$H_2O$ kimberlite so far (Fig. 1) (Golovin et al. 2003, 2007; Kamenetsky et al. 2007a, 2007b, 2012, 2014). Chlorine and water reach 19.3 and 12 wt% in kuliginite and 10.7 and 26 wt% in iowaite, respectively.

Experiments simulating serpentinization processes by Rucklidge and Patterson (1977) showed hydroxychloride to be stabilized by alkaline conditions at the reaction front and to be dissolved subsequently as fresh fluids replace those modified by the production of serpentine. In another experimental study of Poty et al. (1972), alkaline solutions formed after reaction with olivine in the presence of Cl in an originally acidic environment. Synthesis of oxyhydroxides in chlorinated environments by Rémazeilles and Refait (2007) showed strong influence of Cl on the formation of akaganeite $(Fe^{3+},Ni^{2+})_8(OH,O)_{16}Cl_{1.25}\cdot nH_2O$.

In our view, the most realistic scenario for the formation of the discussed mineral assemblages in veins and voids, including kuliginite in olivine-rich kimberlitic types, may be as follows. Percolation of external water, possibly Ca-Cl brines from the aquifer system in the host sediments below 510 m, leads to leaching of primary magmatic chlorides, alkali carbonates, and alkali sulfates, as well as to partial serpentinization of rocks. The latter process causes re-distribution of components in the residual saline fluid in veins and voids. Some water is spent on serpentinization of olivine-rich kimberlites, while the residual fluid becomes enriched in Mg and Fe. Kuliginite and iowaite apparently crystallize from this very residual solution enriched in Mg, Fe, and Cl. Gypsum and NaCl crystallize simultaneously with kuliginite and iowaite. Finds of fluid inclusions in NaCl provide evidence for the hydrothermal origin of NaCl.

According to experimental data Klimchouk (1996), gypsum is unstable above 100 °C even in hydrothermal conditions, and thus the gypsum+kuliginite+iowaite assemblage should crystallize at lower temperatures.

The same temperature can be inferred from the composition of iowaite, which shows complete dehydroxylation at 291 °C in heating experiments Frost et al. (2006), while water contents in iowaite of the analyzed samples correspond to a temperature range within 79 °C. Saini-Eidukat et al. (1994) described hibbingite $Fe_2(OH)_2Cl$ on reinforced steel bars in a swimming pool construction. Other environments where Cl is in contact with Fe-bearing compounds, such as steel in brine, should be checked for the presence of related compounds (Cawthorn et al. 2009). Numerous archaeological studies revealed iron-magnesium hydroxychloride phases on the surface of corroded iron artifacts (Post et al. 2003; Ståhl et al. 2003; Reguer et al. 2007).

## IMPLICATIONS

The presence of two non-serpentinized ultra-fresh kimberlite units in the Udachnaya East kimberlite and available data on melt inclusions in kimberlite minerals offer an exceptional opportunity to study the composition and evolution of kimberlite magma (Golovin et al. 2007, 2017; Kamenetsky et al. 2014; Kitayama et al. 2017; d'Eyrames et al. 2017; Shatskiy et al. 2017).

Finds of halite in some hydrothermally altered kimberlites lead to confusion about the kimberlite origin. The mineral assemblage in this type of kimberlite, which consists of abundant serpentine around lenses and veins, halite, calcite, iowaite,

barite, celestine, gypsum, and kuliginite (Kopylova et al. 2016; this study), has never been reported before for ultra-fresh saline kimberlites (Kamenetsky et al. 2007a, 2007b, 2012, 2014). The occurrence intergrowths of kuliginite and iowaite in halite may trace a hydrothermal/metasomatic process of kimberlite alteration by fluids/brines and metal transport in Cl-bearing solutions. Kuliginite and iowaite intergrowths indicating their simultaneous crystallization at temperatures below 100 °C.

Kuliginite is a new potential constituent of the corrosion system of archaeological iron artifacts buried in soil on a microscopic scale. Therefore, an investigation into Cl-bearing minerals has important implications for preservation of archaeological artifacts and can provide clues to iron corrosion mechanisms.

## Acknowledgments

We greatly appreciate the assistance of our colleagues A.V. Vishnevsky (photographs of minerals), E.N. Nigmatulina (EPMA), and I.V. Pekov (optical properties). The study was supported by state assignment project 0330-2016-0006. Comments by T. Alifirova, constructive reviews by Uwe Kolitsch and an anonymous reviewer, and the associate editor, G. Diego Gatta, helped to improve many aspects of the paper.

## References cited

Alekseev, S.V. (2009) Permafrost-Groundwater Systems of the Yakutian Diamond Province. Akademicheskoe Izdatelstvo "Geo", Novosibirsk.

Alexeev, S.V., Alexeeva, L.P., Borisov, V.N., Shouakar-Stash, O., Frape, S.K., Chabaux, F., and Kononov, A.M. (2007) Isotopic composition (H, O, Cl, Sr) of ground brines of the Siberian Platform. Russian Geology and Geophysics, 48, 225–236.

Aullon, G., Bellamy, D., Orpen, A.G., Brammer, L., Bruton, F., and Eric, A. (1998) Metal-bound chlorine often accepts hydrogen bonds. Chemical Communications. Royal Society of Chemistry, 6, 653–654.

Braithwaite, R.S.W., Dunn, P.J., Pritchard, R.G., and Parr, W.H. (1994) Iowaite, a re-investigation. Mineralogical Magazine, 58, 77–86.

Braithwaite, R., Mereiter, K., Paar, W., and Clark, A. (2011) Herbertsmithite, $Cu_3Zn(OH)_6Cl_2$, a new species, and the definition of paratacamite. Mineralogical Magazine, 68, 527–539.

Brakhfogel, F.F. (1984) Geological aspects of kimberlite magmatism in the northeastern Siberian platform. Siberian Branch of Academy of Sciences of USSR, 128, 130–135.

Brese, N.E., and O'Keeffe, M. (1991) Bond-valence parameters for solids. Acta Crystallographica, B47, 192–197

Cawthorn, R.G., Luvhimbe, C., and Slabbert, M. (2009) Suspected presence of hibbingite in olivine pyroxenite adjacent to the UG2 chromitite, Bushveld Complex, South Africa. Canadian Mineralogist, 47, 1075–1085.

Clissold, M.E., Leverett, P., Williams, P.A., Hibbs, D.E., and Nickel, E.H. (2007) The structure of gillardite, the Ni-analogue of herbertsmithite, from Widgiemooltha, Western Australia. Canadian Mineralogist, 45, 317–320.

Crichton, W.A., and Müller, H. (2017) Centennialite, $CaCu_3(OH)_6Cl_2 \cdot nH_2O$, n = 0.7, a new kapellasite-like species, and a reassessment of calumetite. Mineralogical Magazine, 81, 1105–1124.

Davis, G.L., Sobolev, N.V., and Kharkiv, A.D. (1980) New data on the age of Yakutian kimberlites obtained by uranium-lead study of zircons. Doklady Akademii Nauk SSSR, 254, 175–179, (in Russian).

d'Eyrames, E., Thomassot, E., Kitayama, Y., Golovin, A., Korsakov, A., and Ionov, D. (2017) A mantle origin for sulfates in the unusual salty Udachnaya—East kimberlite from sulfur abundances, speciation and their relationship with groundmass carbonates. Bulletin de la Société géologique de France, 188, 1–8.

Drozdov, A.V., Egorov, K.N., Gotovtsev, S.P., and Klimovsky, I.V. (1989) Hydrogeological structure and hydrochemical zonation of the Udachnaya kimberlite pipe. In Combined Permafrost and Hydrogeological Studies, p. 146–155. Institute of Permafrost Siberian Branch of Academy of Sciences, Yakutsk.

Foord, E.E., and Mills, B.A. (1978) Biaxiality in 'isometric' and 'dimetric' crystals. American Mineralogist, 63, 316–325.

Frost, R., Bouzaid, J., Musumeci, A., Kloprogge, J., and Martens, W. (2006) Thermal decomposition of the synthetic hydrotalcite iowaite. Journal of Thermal Analysis and Calorimetry, 86, 437–441.

Frost, R.L., Adebajo, M.O., and Erickson, K.L. (2005) Raman spectroscopy of synthetic and natural iowaite. Spectrochimica Acta Part A: Molecular and Biomolecular Spectroscopy, 61, 613–620.

Golovin, A.V., Sharygin, V.V., Pokhilenko, N.P., Malkovets, V.G., Kolesov, B.A., and Sobolev, N.V. (2003) Secondary melt inclusions in olivine from unaltered kimberlites of the Udachnaya-East pipe, Yakutia. Doklady Earth Sciences, 388, 93–96.

Golovin, A.V., Sharygin, V.V., and Pokhilenko, N.P. (2007) Melt inclusions in olivine phenocrysts in unaltered kimberlites from the Udachnaya-East pipe, Yakutia: Some aspects of kimberlite magma evolution during late crystallization stages. Petrology, 15, 168–183.

Golovin, A.V., Sharygin, I.S., and Korsakov, A.V. (2017) Origin of alkaline carbonates in kimberlites of the Siberian craton: Evidence from melt inclusions in mantle olivine of the Udachnaya-East pipe. Chemical Geology, 455, 357–375.

Hålenius, U., Hatert, F., Pasero, M., and Mills, S. (2016) IMA Commission on New Minerals, Nomenclature and Classification (CNMNC) Newsletter 33. New minerals and nomenclature modifications approved in 2016. Mineralogical Magazine, 80, 1135–1144.

Hamilton, W.C. (1965) Significance tests on the crystallographic R factor. Acta Crystallographica, 18, 502–510.

Hawthorne, F. (1985) Refinement of the crystal structure of botallackite. Mineralogical Magazine, 49, 87–91.

Kahr, B., and McBride, J.M. (1992) Optically anomalous crystals. Angewandte Chemie International Edition, 31, 1–26.

Kamenetsky, M.B., Sobolev, A.V., Kamenetsky, V.S., Maas, R., Danyushevsky, L.V., Thomas, R., Pokhilenko, N.P., and Sobolev, N.V. (2004) Kimberlite melts rich in alkali chlorides and carbonates: a potent metasomatic agent in the mantle. Geology, 32, 845–848.

Kamenetsky, V.S., Sharygin, V.V., Kamenetsky, M.B., and Golovin, A.V. (2006) Chloride-carbonate nodules in kimberlites from the Udachnaya pipe: alternative approach to the evolution of kimberlite magmas. Geochemistry International, 44, 935–940.

Kamenetsky, V.S., Kamenetsky, M.B., Sharygin, V.V., Faure, K., and Golovin, A.V. (2007a) Chloride and carbonate immiscible liquids at the closure of the kimberlite magma evolution (Udachnaya-East kimberlite, Siberia). Chemical Geology, 237, 384–400.

Kamenetsky, V.S., Kamenetsky, M.B., Sobolev, A.V., Golovin, A.V., Demouchy, S., Faure, K., Sharygin, V.V., and Kuzmin, D.V. (2007b) Olivine in the Udachnaya-East kimberlite (Yakutia, Russia): types, compositions and origins. Journal of Petrology, 49, 823–839.

Kamenetsky, V.S., Kamenetsky, M.B., Weiss, Y., Navon, O., Nielsen, T.F., and Mernagh, T.P. (2009) How unique is the Udachnaya-East kimberlite? Comparison with kimberlites from the Slave Craton (Canada) and SW Greenland. Lithos, 112, 334–346.

Kamenetsky, V.S., Kamenetsky, M.B., Golovin, A.V., Sharygin, V.V., and Maas, R. (2012) Ultrafresh salty kimberlite of the Udachnaya–East pipe (Yakutia, Russia): A petrological oddity or fortuitous discovery? Lithos, 152, 173–186.

Kamenetsky, V.S., Golovin, A.V., Maas, R., Giuliani, A., Kamenetsky, M.B., and Weiss, Y. (2014) Towards a new model for kimberlite petrogenesis: Evidence from unaltered kimberlites and mantle minerals. Earth-Science Reviews, 139, 145–167.

Kampf, A.R., Sciberras, M.J., Leverett, P., Williams, P.A., Malcherek, T., Schlüter, J., Welch, M.D., Dini, M., and Donoso, A.M. (2013a) Paratacamite-(Mg), $Cu_3(Mg, Cu)Cl_2(OH)_6$; a new substituted basic copper chloride mineral from Camerones, Chile. Mineralogical Magazine, 77, 3113–3124.

Kampf, A.R., Sciberras, M.J., Williams, P.A., Dini, M., and Donoso, A. (2013b) Leverettite from the Torrecillas mine, Iquique Provence, Chile: the Co-analogue of herbertsmithite. Mineralogical Magazine, 77, 3047–3054.

Kharkiv, A.D., Zinchuk, N.N., and Kryuchkov, A.I. (1998) Primary Diamond Deposits of the World, 555 p. Nedra, Moscow.

Kinny, P.D., Griffin, B.J., Heaman, L.M., Brakhfogel, F.F., and Spetsius, Z.V. (1997) SHRIMP U-Pb ages of perovskite from Yakutian kimberlites. Russian Geology and Geophysics, 38, 97–105.

Kitayama, Y., Thomassot, E., Galy, A., Golovin, A., Korsakov, A., d'Eyrames, E., Assayag, N., Bouden, N., and Ionov, D. (2017) Co-magmatic sulfides and sulfates in the Udachnaya-East pipe (Siberia): A record of the redox state and isotopic composition of sulfur in kimberlites and their mantle sources. Chemical Geology, 455, 315–330.

Klimchouk, A. (1996) The dissolution and conversion of gypsum and anhydrite. International Journal of Speleology, 25, 2–16.

Kopylova, M.G., Gaudet, M., Kostrovitsky, S.I., Polozov, A.G., and Yakovlev, D.A. (2016) Origin of salts and alkali carbonates in the Udachnaya East kimberlite: Insights from petrography of kimberlite phases and their carbonate and evaporite xenoliths. Journal of Volcanology and Geothermal Research, 327, 116–134.

Kozlov, I., and Levshov, P. (1962) Amakinite, a new mineral of the brucitepyrochroite group. American Mineralogist, 47, 1218.

Krause, W., Bernhardt, H.-J., Braithwaite, R.S.W., Kolitsch, U., and Pritchard, R. (2006) Kapellasite, $Cu_3Zn(OH)_6Cl_2$, a new mineral from Lavrion, Greece, and its crystal structure. Mineralogical Magazine, 70, 329–340.

Libowitzky, E. (1999) Correlation of OH stretching frequencies and OH···O hydrogen bond lengths in minerals. Monatshefte für Chemie, 130, 1047–1059.

Maas, R., Kamenetsky, M.B., Sobolev, A.V., Kamenetsky, V.S., and Sobolev, N.V. (2005) Sr, Nd, and Pb isotope evidence for a mantle origin of alkali chlorides and carbonates in the Udachnaya kimberlite, Siberia. Geology, 33, 549–552.

Malcherek, T., and Schlüter, J. (2009) Structures of the pseudo-trigonal polymorphs of $Cu_2(OH)_3Cl$. Acta Crystallographica, B65, 334–341.

Malcherek, T., Bindi, L., Dini, M., Ghiara, M., Donoso, A.M., Nestola, F., Rossi,

M., and Schlüter, J. (2014) Tondiite, $Cu_3Mg(OH)_6Cl_2$, the Mg-analogue of herbertsmithite. Mineralogical Magazine, 78, 583–590.
Marshintsev, V.K., Migalkin, K.N., Nikolaev, N.S., and Barashkov, I.P. (1976) Unchanged kimberlite of Udachnaya-Vostochnaya pipe. Doklady Akademii Nauk SSSR, 231, 961–964.
Mascal, M. (1997) A statistical analysis of halide H–A (A= OR, NR 2, N+ R 3) hydrogen bonding interactions in the solid state. Journal of the Chemical Society, Perkin Transactions, 2, 10, 1999–2001.
Mernagh, T.P., Kamenetsky, V.S., and Kamenetsky, M.B. (2011) A Raman microprobe study of melt inclusions in kimberlites from Siberia, Canada, SW Greenland and South Africa. Spectrochimica Acta Part A: Molecular and Biomolecular Spectroscopy, 80, 82–87.
Momma, K., and Izumi, F. (2011) VESTA 3 for three-dimensional visualization of crystal, volumetric and morphology data. Journal of Applied Crystallography, 44, 1272–1276.
Nishio-Hamane, D., Momma, K., Ohnishi, M., Shimobayashi, N., Miyawaki, R., Tomita, N., Okuma, R., Kampf, A., and Minakawa, T. (2017) Iyoite, $MnCuCl(OH)_3$ and misakiite, $Cu_3Mn(OH)_6Cl_2$: new members of the atacamite family from Sadamisaki Peninsula, Ehime Prefecture, Japan. Mineralogical Magazine, 81, 485–498.
Palatinus, L., and Chapuis, G. (2007) SUPERFLIP—a computer program for the solution of crystal structures by charge flipping in arbitrary dimensions. Journal of Applied Crystallography, 40, 786–790.
Parise, J.B., and Hyde, B.G. (1986) The structure of atacamite and its relationship to spinel. Acta Crystallographica, C42, 1277–1280.
Petrıcek, V., Dusek, M., and Palatinus, L. (2014) Crystallographic computing system JANA2006: general features. Zeitschrift für Kristallographie: Crystalline Materials, 229, 345–352.
Post, J.E., Heaney, P.J., Dreele, R.B.V., and Hanson, J.C. (2003) Neutron and temperature-resolved synchrotron X-ray powder diffraction study of akaganéite. American Mineralogist, 88, 782–788.
Poty, B., Holland, H.D., and Borcsik, M. (1972) Solution-mineral equilibria in the system $MgO\text{-}SiO_2\text{-}H_2O\text{-}MgCl_2$ at 500°C and 1 kbar. Geochimica et Cosmochimica Acta, 36, 1101–1113.
Reguer, S., Neff, D., Bellot-Gurlet, L., and Dillmann, P. (2007) Deterioration of iron archaeological artefacts: micro-Raman investigation on Cl-containing corrosion products. Journal of Raman Spectroscopy, 38, 389–397.
Rémazeilles, C., and Refait, P. (2007) On the formation of β-FeOOH (akaganéite) in chloride-containing environments. Corrosion Science, 49, 844–857.
Rogers, A.F. (1924) Kempite, a new manganese mineral from California. American Journal of Science, 44, 145–150.
Rucklidge, J.C., and Patterson, G.C. (1977) The role of chlorine in serpentinization. Contributions to Mineralogy and Petrology, 65, 39–44.
Saini-Eidukat, B., Kucha, H., and Keppler, H. (1994) Hibbingite, $Fe_2(OH)_3Cl$, a new mineral from the Duluth Complex, Minnesota, with implications for the oxidation of Fe-bearing compounds and the transport of metals. American Mineralogist, 79, 555–561.
Sciberras, M.J., Leverett, P., Williams, P.A., Hibbs, D.E., Downes, P.J., Welch, M.D., and Kampf, A.R. (2013) Paratacamite-(Ni),$Cu_3(Ni,Cu)Cl_2(OH)_6$, a new mineral from the Carr Boyd Rocks mine, Western Australia. Australian Journal of Mineralogy, 17, 39–44.
Shatskiy, A., Litasov, K.D., Sharygin, I.S., and Ohtani, E. (2017) Composition of primary kimberlite melt in a garnet lherzolite mantle source: constraints from melting phase relations in anhydrous Udachnaya-East kimberlite with variable $CO_2$ content at 6.5 GPa. Gondwana Research, 45, 208–227.
Shtukenberg, A., and Punin, Y.O. (2007) Stress induced optical anomalies. In A. Shtukenberg and Y. Shtukenberg, and Kahr, Eds., Optically Anomalous Crystal, p. 35–94. Springer.
Smith, B.H.S., Nowicki, T.E., Russell, J.K., Webb, K.J., Mitchell, R.H., Hetman, C.M., Harder, M., Skinner, E., and Robey, J.A. (2013) Kimberlite terminology and classification. In D.G. Pearson and H.S. Grütter, Eds., Proceedings of 10th International Kimberlite Conference, p. 1–17. Springer.
Ståhl, K., Nielsen, K., Jiang, J., Lebech, B., Hanson, J.C., Norby, P., and van Lanschot, J. (2003) On the akaganéite crystal structure, phase transformations and possible role in post-excavational corrosion of iron artifacts. Corrosion Science, 45, 2563–2575.
Steiner, T. (1998) Hydrogen-bond distances to halide ions in organic and organometallic crystal structures: up-to-date database study. Acta Crystallographica, B54, 456–463.
Welch, M.D., Sciberras, M.J., Williams, P.A., Leverett, P., Schlüter, J., and Malcherek, T. (2014) A temperature-induced reversible transformation between paratacamite and herbertsmithite. Physics and Chemistry of Minerals, 41, 33–48.
Yudin, D.S., Tomilenko, A.A., Alifirova, T.A., Travin, A.V., Murzintsev, N.G., and Pokhilenko, N.P. (2011) Results of $^{40}Ar/^{39}Ar$ dating of phlogopites from kelyphitic rims around garnet grains (Udachnaya-Vostochnaya kimberlite pipe). Doklady Earth Sciences, 469, 728–731.

Manuscript received November 3, 2017
Manuscript accepted May 11, 2018
Manuscript handled by G. Diego Gatta

## Endnote:

[1]Deposit item AM-18-86363, Supplemental Tables and CIF. Deposit items are free to all readers and found on the MSA web site, via the specific issue's Table of Contents (go to http://www.minsocam.org/MSA/AmMin/TOC/2018/Sep2018_data/Sep2018_data.html).